Exciton polaritons in transition-metal dichalcogenides and their direct excitation via energy transfer

Yuri N. Gartstein,[1,*] Xiao Li,[1,2,†] and Chuanwei Zhang[1,‡]
[1]*Department of Physics, The University of Texas at Dallas, Richardson, Texas, 75080, USA*
[2]*Department of Physics, The University of Texas at Austin, Austin, Texas 78712, USA*
(Received 28 January 2015; revised manuscript received 30 July 2015; published 28 August 2015)

Excitons, composite electron-hole quasiparticles, are known to play an important role in optoelectronic phenomena in many semiconducting materials. Recent experiments and theory indicate that the band-gap optics of the newly discovered monolayer transition-metal dichalcogenides (TMDs) is dominated by tightly bound valley excitons. The strong interaction of excitons with long-range electromagnetic fields in these two-dimensional systems can significantly affect their intrinsic properties. Here, we develop a semiclassical framework for intrinsic exciton polaritons in monolayer TMDs that treats their dispersion and radiative decay on the same footing and can incorporate effects of the dielectric environment. It is demonstrated how both inter- and intravalley long-range interactions influence the dispersion and decay of the polaritonic eigenstates. We also show that exciton polaritons can be efficiently excited via resonance energy transfer from quantum emitters such as quantum dots, which may be useful for various applications.

DOI: 10.1103/PhysRevB.92.075445 PACS number(s): 78.20.Bh, 78.60.Fi, 78.66.Qn, 78.68.+m

I. INTRODUCTION

Monolayer molybdenum disulfide MoS_2 and other group-VI transition-metal dichalcogenides (TMDs) are novel two-dimensional (2D) semiconductor systems whose electronic and optical properties attract a great deal of attention [1–29]. One of their prominently discussed features is the opportunity to manipulate the valley degree of freedom, including by optical means due to opposite-handed circular polarizations of the interband transitions in the two valleys [4]. Growing experimental and theoretical evidence [2–8,17–29] indicates that the band-gap optical properties of monolayer TMDs are dominated by relatively tightly bound electron-hole pairs, excitons, with binding energies substantially larger than in the majority of conventional inorganic semiconductor quantum wells [30,31]. The corresponding 2D exciton physics in TMDs may therefore reflect generally stronger interactions of excitons with macroscopic electric fields and light. In fact, experimental evidence of strong coupling between MoS_2 excitons and dielectric microcavity photons has been recently reported [32].

An important fundamental issue is the nature of intrinsic excitonic eigenstates and their energy-momentum (dispersion) relationships. It is these relationships that are of particular interest to us here. It was emphasized recently [23] that the long-range exchange Coulomb interaction mixes individual valley excitons to establish excitons with the longitudinal (L) and transverse (T) polarizations as normal system modes, similar to quantum well excitons [33,34]. It was also suggested [23] that the resulting exciton spectrum, as a function of its center-of-mass in-plane wave vector $\mathbf{k} = (k_x, k_y) = k(\cos\theta, \sin\theta)$, would exhibit a specific Dirac-cone-like behavior at low momenta $\hbar k$, in particular within the light cone, $k < \kappa = \omega/c$.

In this paper [35] we address the issue of the exciton dispersion at small k as affected exclusively by long-range (or macroscopic) interactions. Consistent with this end, a semiclassical analysis is performed of the interaction of monolayer excitons with long-range electromagnetic fields. Our results show that (1) the dispersion of L and T excitons is affected by *both* inter- and intravalley interaction processes leading to the overall generic behavior characteristic of the 2D excitons [33,34,36,37]. That behavior does not exhibit a Dirac-cone feature. In the electrostatic limit, this can be seen already from the Coulomb interaction calculations as illustrated below and was recently [29] recognized. While the dispersion of L excitons is indeed substantially altered, the effect on the dispersion of T excitons would be inconsistent with the electrostatics of the transverse polarization waves. (2) Moreover, also in a general fashion, we demonstrate that the *intrinsic* behavior of excitations within and in the vicinity of the light cone would be that of the 2D exciton polaritons as determined by the full electromagnetic (rather than just electrostatic [23]) coupling of valley excitons taking into account the retardation effects [31,37] With this approach, both renormalization of the excitonic bands and the exciton radiative decay appear on the same footing as a consequence of the exciton interaction with macroscopic electromagnetic fields. Consequently, general features of the intrinsic exciton polaritons are particularly clearly accentuated in the macroscopic electrodynamics framework. It allows one, for instance, to straightforwardly generalize the analysis of the polariton dispersion and radiative decay in free-standing monolayer TMDs to monolayers at the interface between different media that we discuss in this paper. Such a framework would also be applicable to more involved photonic structures with TMDs that can be of interest for optoelectronic applications. In another example, we use that framework here to illustrate the possibility of very efficient direct excitation of monolayer polaritons by energy transfer from proximal electric-dipole emitters. Energy transfer from quantum dots to MoS_2 has been observed experimentally [38,39], this process is also considered of potential importance for practical applications.

*yuri.gartstein@utdallas.edu
†Present address: Condensed Matter Theory Center, Department of Physics, University of Maryland, College Park, Maryland 20742, USA.
‡chuanwei.zhang@utdallas.edu

II. EXCITON POLARITONS FROM EFFECTIVE DIPOLE-DIPOLE INTERACTIONS

In a common basic description of optically active lowest energy excitons in monolayer TMDs, they arise as a result of the direct Coulomb attraction between an electron and a hole in the same valley. Due to the strong spin-orbit coupling in TMDs, the electron-hole spin composition is associated with the valley [4] and therefore we will be omitting spin indices. In the valley-based picture there are then two exciton species (index $\alpha = 1,2$) corresponding to two different valleys, both having the same energy dispersion

$$E_0(\mathbf{k}) = \hbar\omega_0(k) = \hbar\omega_0 + \hbar^2 k^2/2M_0, \tag{1}$$

where $\hbar\omega_0$ is typically somewhat below 2 eV and the exciton mass M_0 is close to the free electron's m_e [8,10,19,23] The parabolic kinetic energy in Eq. (1) with M_0 being the sum of electron and hole effective masses signifies the fact that the exciton propagation in space is enabled by the simultaneous motion of the electron and hole. The inclusion of the standard exchange Coulomb interaction results in another mechanism of the exciton propagation and concomitant modifications of its dispersion, which can be seen as the electric field of the exciton annihilated at one spatial point creating the exciton at another point. Such a long-range process corresponds to the effective electrostatic dipole-dipole coupling, which is a well-known major exciton transport mechanism in molecular systems [37]. To briefly outline this picture for the generic continuum description of excitons as relevant to our application here, consider the electron-electron Coulomb interaction

$$U = \frac{1}{2}\int d\mathbf{r}_1 d\mathbf{r}_2 \psi^\dagger(\mathbf{r}_1)\psi^\dagger(\mathbf{r}_2)U_C(\mathbf{r}_1-\mathbf{r}_2)\psi(\mathbf{r}_2)\psi(\mathbf{r}_1), \tag{2}$$

where the electron annihilation operator

$$\psi(\mathbf{r}) = \sum_{\alpha\mu}\psi_{\alpha\mu}(\mathbf{r}) = \sum_{\alpha\mu\mathbf{q}} a_{\alpha\mu,\mathbf{q}}\phi^\alpha_{\mu\mathbf{q}}(\mathbf{r}) \tag{3}$$

is associated with the sum over valleys ($\alpha = 1,2$) and bands (conduction, $\mu = c$, and valence, $\mu = v$). Further expansion in Eq. (3) is over electron operators $a_{\alpha\mu,\mathbf{q}}$ with wave vectors $\mathbf{q}$ and Bloch wave functions $\phi^\alpha_{\mu\mathbf{q}}(\mathbf{r})$. For a uniformly screened Coulomb repulsion, $U_C(\mathbf{r}_1-\mathbf{r}_2) = e^2/\varepsilon|\mathbf{r}_1-\mathbf{r}_2|$, where e is the electron charge and ε the effective dielectric constant, but the screening could also be distance dependent. The peculiarities of screening effects in (quasi) 2D systems and applications to TMDs have been discussed in Ref. [22].

In accordance with representation (3), the integrand in interaction (2) contains terms like

$$\psi^\dagger_{\alpha c}(\mathbf{r}_1)\psi^\dagger_{\beta v}(\mathbf{r}_2)U_C(\mathbf{r}_1-\mathbf{r}_2)\psi_{\beta v}(\mathbf{r}_2)\psi_{\alpha c}(\mathbf{r}_1)$$

featuring density operators $\psi^\dagger_{\alpha\mu}(\mathbf{r})\psi_{\alpha\mu}(\mathbf{r})$ and related to the direct Coulomb interaction between an electron and a hole. Valley excitons are bound states that are formed as a result of this direct interaction:

$$|\alpha\mathbf{k}\rangle = \sum_{\mathbf{q}}\Phi_{\mathbf{q}}a^\dagger_{\alpha c,\mathbf{q}}a_{\alpha v,\mathbf{q}-\mathbf{k}}|\text{g.s.}\rangle \tag{4}$$

for excitons with wave vector $\mathbf{k}$ and energy (1). Here $|\text{g.s.}\rangle$ is the ground state, whereas excitonic state (4) is a linear combination of band electron-hole pair states with the momentum-space wave function $\Phi_{\mathbf{q}}$. For the continuum excitonic states in the effective mass approximation (1), the wave vectors $\mathbf{q}$ in Eq. (4) are assumed to be measured relative to the position of band edges ($\mathbf{K}_\alpha$ points) in the respective valleys and are small. One immediately recognizes the known relationship $\sum_{\mathbf{q}}\Phi_{\mathbf{q}} = \sqrt{\mathcal{V}}\phi(0)$ that is employed below. Here $\mathcal{V}$ is the system volume and $\phi(0)$ the real-space wave function of the relative electron-hole motion for their coinciding position. We note that the precise knowledge of the exciton wave function and the exciton binding energy is not essential for the effects that we focus on in this paper. We refer the reader to Ref. [22], which summarizes and discusses several theoretical calculations of the excitons in MoS_2 with a particular emphasis on the effects of the screening.

A different type of contribution to the integrand of Eq. (2) is exemplified by the expression

$$\psi^\dagger_{\alpha c}(\mathbf{r}_1)\psi^\dagger_{\beta v}(\mathbf{r}_2)U_C(\mathbf{r}_1-\mathbf{r}_2)\psi_{\beta c}(\mathbf{r}_2)\psi_{\alpha v}(\mathbf{r}_1),$$

which features interband *transitional* density operators like $\rho^\alpha_{cv}(\mathbf{r}) = \psi^\dagger_{\alpha c}(\mathbf{r})\psi_{\alpha v}(\mathbf{r})$ and corresponds to the exchange Coulomb interaction (U^{exch}) for the excitonic states. These types of terms would then lead to corrections to exciton energies (1) via matrix elements

$$U^{\text{exch}}_{\alpha\beta}(\mathbf{k}) = \langle\alpha\mathbf{k}|U^{\text{exch}}|\beta\mathbf{k}\rangle. \tag{5}$$

The interband transitional densities can be readily related to the interband electric-dipole polarization $\mathbf{P}$ in the continuum description we are interested in by using the $\mathbf{k}\cdot\mathbf{p}$ theory [30,31] expansion of Bloch wave functions in the vicinity of the conduction and valence band edges. Restricting, for clarity, to the two bands in each valley, the valence band functions

$$\phi^\alpha_{v\mathbf{q}}(\mathbf{r}) = \frac{1}{\sqrt{\mathcal{V}}}e^{i\mathbf{q}\cdot\mathbf{r}}\left[u^\alpha_v(\mathbf{r}) - \frac{\mathbf{q}\cdot\mathbf{p}^\alpha_{cv}}{m_e E_g}u^\alpha_c(\mathbf{r})\right], \tag{6}$$

where E_g is the energy band gap and $\mathbf{p}^\alpha_{cv}$ the interband matrix element of the electron momentum operator. The latter determines the admixture of the conduction-band-edge periodic Bloch functions $u^\alpha_c(\mathbf{r})$ into the valence-band-edge periodic functions $u^\alpha_v(\mathbf{r})$. Using Eq. (6) and the analogous expression for the conduction band states

$$\phi^\alpha_{c\mathbf{q}}(\mathbf{r}) = \frac{1}{\sqrt{\mathcal{V}}}e^{i\mathbf{q}\cdot\mathbf{r}}\left[u^\alpha_c(\mathbf{r}) + \frac{\mathbf{q}\cdot\mathbf{p}^\alpha_{vc}}{m_e E_g}u^\alpha_v(\mathbf{r})\right], \tag{7}$$

the macroscopic (over distances substantially larger than the unit cell) averaging eliminates the periodic functions from consideration and emphasizes the envelope functions. For the transitional charge density operator $e\rho^\alpha_{cv}$, e.g., this results in

$$e\rho^\alpha_{cv}(\mathbf{r}) \to -\nabla\cdot\mathbf{P}^\alpha_{cv}(\mathbf{r}), \tag{8}$$

where the macroscopic interband polarization operator

$$\mathbf{P}^\alpha_{cv}(\mathbf{r}) = \frac{1}{\mathcal{V}}\sum_{\mathbf{q}_1\mathbf{q}_2}a^\dagger_{\alpha c,\mathbf{q}_2}a_{\alpha v,\mathbf{q}_1}e^{i(\mathbf{q}_1-\mathbf{q}_2)\mathbf{r}}\,\mathbf{d}^\alpha_{cv}, \tag{9}$$

and the (optical) interband electric-dipole transition matrix element

$$\mathbf{d}^{\alpha}_{cv} = -ie\mathbf{p}^{\alpha}_{cv}/m_e E_g \tag{10}$$

for electron-hole pair creation in valley α is traditionally [31] related to the momentum matrix element. The described framework applies to systems of different dimensionalities with the proper definition of volume $\mathcal{V}$ and of Cartesian coordinates in spatial vectors $\mathbf{r}$ and spatial derivatives of operator $\boldsymbol{\nabla}$.

With association (8) in place, it is clear from standard electrostatics [40] that the long-range exchange Coulomb interaction indeed corresponds to the electrostatic dipole-dipole coupling. Matrix elements (5) can thus be directly represented by using Eqs. (9) and (4) in terms of interacting "transition dipoles" [Eq. (10)]. This physically attractive real-space picture can then be readily extended to the dipole-dipole coupling mediated by the full electromagnetic interactions including the retardation effects. The resulting intrinsic excitations, known as exciton polaritons, would thus take into account the exciton-light interaction [31,36,37] that is absent in the picture of Coulomb excitons derived with electrostatic interactions alone. It was demonstrated [41] that the dipole-dipole calculations with the retarded fields result in the same exciton polaritons as arising from the more familiar treatment [31,37] of the interaction of Coulomb excitons with transverse photons [see a schematic picture in Fig. 1(c)]. Since the full electromagnetic interaction depends also on the frequency (energy), it is more accurate to discuss the results in terms of exciton self-energy corrections $\boldsymbol{\Sigma}$ that can be used in the self-consistent calculations of the exciton Green's functions in the Dyson equation: $\mathbf{G} = \mathbf{G}_0 + \mathbf{G}_0\boldsymbol{\Sigma}\mathbf{G}$.

It is convenient to classify the electromagnetic interactions in monolayer TMDs as intravalley ($\alpha = \beta$) and intervalley ($\alpha \neq \beta$) couplings, in some analogy with bipartite lattices and molecular systems with two molecules per unit cell [37]. Consequently, the exciton Green's functions $\mathbf{G}$ and exciton self-energy correction $\boldsymbol{\Sigma}$ due to the interactions are 2×2 matrices, the noninteracting $\mathbf{G}_0$ being just a diagonal matrix corresponding to valley excitons with energies (1). Matrix elements of $\boldsymbol{\Sigma}$ are evaluated precisely as we described above for Eq. (5) with the understanding that the electrostatic interaction of transition dipoles can be replaced by the full interaction. We therefore write the result in a general form that emphasizes this interaction:

$$\Sigma_{\alpha\beta}(E,\mathbf{k}) = \int d\mathbf{r}\, v_{\alpha\beta}(\mathbf{r})\, e^{i\mathbf{k}\cdot\mathbf{r}}. \tag{11}$$

It is a function of wave vector $\mathbf{k}$ but can also be a function of energy variable $E = \hbar\omega = \hbar c\kappa$ implicitly present in energy density $v(\mathbf{r})$ in the integrand. The energy density $v_{\alpha\beta}(\mathbf{r}) = |\phi(0)|^2\, V_{\alpha\beta}(\mathbf{r})$ is determined by the probability $|\phi(0)|^2$ to find the electron and hole of the exciton at the same spatial point and by the dipole-dipole interaction matrix elements $V_{\alpha\beta}(\mathbf{r})$. For the standard 2D Wannier-Mott excitons [31], $|\phi(0)|^2 = 8/(\pi a_B^2)$; and *ab initio* calculations [8,11,21,25] estimate the exciton Bohr radius in monolayer TMDs as $a_B \sim 1$ nm. The dipole-dipole interaction is of course dependent on the relative dipole position $\mathbf{r} = r\hat{\mathbf{r}}$ and their orientations but is also a function of the transition ("dipole oscillation") frequency

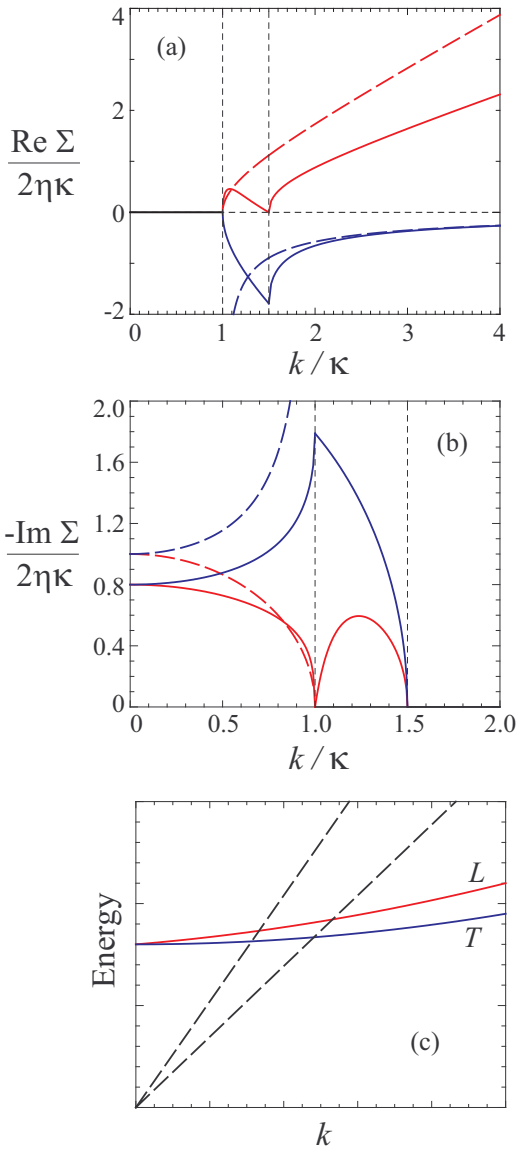

FIG. 1. (Color online) Functional behavior of the (a) real and (b) imaginary parts of the intrinsic exciton-polariton self-energy as per Eqs. (17) and (21) for a fixed value of the vacuum light wave number κ. Red color lines are used for the longitudinal (L) and blue for the transverse (T) polaritons. Shown with dashed lines are the results for a free-standing monolayer in vacuum, and solid lines are for the monolayer on a glasslike substrate, see text. (c) Schematically, not to scale: Dispersion of the longitudinal and transverse Coulomb excitons as renormalized by the electrostatic Coulomb interaction. At the interface between two media with different refraction indices, Coulomb excitons would be interacting with the transverse photons of the media, whose dispersion is shown by dashed lines.

when the retardation is taken into account. Indeed, for the free-standing monolayers in vacuum the standard long-range part of the interaction would acquire a form of

$$V_{\alpha\beta}(\mathbf{r}) = \frac{e^{i\kappa r}}{r}\left\{\kappa^2\left[\left(\hat{\mathbf{r}}\cdot\mathbf{d}^{\alpha}_{cv}\right)\left(\hat{\mathbf{r}}\cdot\mathbf{d}^{\beta}_{vc}\right) - \mathbf{d}^{\alpha}_{cv}\cdot\mathbf{d}^{\beta}_{vc}\right] + \left(\frac{1}{r^2} - \frac{i\kappa}{r}\right)\left[\mathbf{d}^{\alpha}_{cv}\cdot\mathbf{d}^{\beta}_{vc} - 3\left(\hat{\mathbf{r}}\cdot\mathbf{d}^{\alpha}_{cv}\right)\left(\hat{\mathbf{r}}\cdot\mathbf{d}^{\beta}_{vc}\right)\right]\right\} \tag{12}$$

as arising from the full electromagnetic dipole-dipole coupling (in Gaussian units) [40]. The energy dependence of the interaction (12) is manifest via the light vacuum wave number $\kappa = \omega/c$; it disappears in the familiar electrostatic limit of $\kappa \to 0$ (speed of light $c \to \infty$). The interacting α and β species in Eq. (12) are represented by the corresponding interband dipole transition matrix elements (10) for creation, $\mathbf{d}^{\alpha}_{cv}$, and annihilation, $\mathbf{d}^{\beta}_{vc}$, of electron-hole pairs. Both vectors $\mathbf{r}$ and transition dipoles are in-plane vectors for the monolayer TMD. In the electrostatic limit, the self-energy corrections (11) would be reduced to Eq. (5) and become real valued and functions of wave vector $\mathbf{k}$ only. With the retarded electric fields, however, $\Sigma_{\alpha\beta}$ are functions of both energy and wave-vector variables and generally complex valued; they would therefore determine both the exciton dispersion and the decay width (decay into photons) in a self-consistent calculation.

The in-plane interband dipole transition matrix elements $\mathbf{d}^{\alpha}_{cv} = (d^{(\alpha)}_x, i d^{(\alpha)}_y)$ have a common form for both valleys but with the opposite handedness of their circular polarization:

$$d^{(1)}_x = d^{(1)}_y = d^{(2)}_x = -d^{(2)}_y = \mathcal{D}, \tag{13}$$

where we chose $\mathcal{D}$ as a real positive quantity. From a two-band monolayer TMD model [4], for instance, the dipole transition moment would be $\mathcal{D} = eat/E_g$, where a is the lattice structure constant ($\simeq$3.19 Å), t the nearest-neighbor hopping integral ($\simeq$1.10 eV), and E_g the conduction-valence energy band gap. A calculation based on the three-band model [24] gives the same form, but with a slightly different value of t.

The difference between the transition dipole moments (13) in the two valleys translates into the difference of inter- and intravalley couplings (12). A direct calculation of integrals in Eq. (11) then leads [42] to the following dependence of the self-energy matrix on wave vector $\mathbf{k} = k(\cos\theta, \sin\theta)$:

$$\mathbf{\Sigma}(E,\mathbf{k}) = \begin{pmatrix} J_0 & \exp(2i\theta)\, J_1 \\ \exp(-2i\theta)\, J_1 & J_0 \end{pmatrix}, \tag{14}$$

where the intravalley component

$$J_0 = -i\eta(\sqrt{\kappa^2 - k^2} + \kappa^2/\sqrt{\kappa^2 - k^2}) \tag{15}$$

and the intervalley component

$$J_1 = i\eta k^2/\sqrt{\kappa^2 - k^2} \tag{16}$$

feature the same magnitude scale $\eta = 2\pi|\phi(0)|^2\mathcal{D}^2$. The functional form of these components illustrates the great qualitative distinction resulting from the retarded interactions: the obtained corrections J_0 and J_1 are purely imaginary above the light line, $k < \kappa$, but become purely real ($\sqrt{\kappa^2 - k^2} \to i\sqrt{k^2 - \kappa^2}$) below the light line, $k > \kappa$. As is known [36,37], this signifies the impossibility for the intrinsic 2D exciton polariton with $k > \kappa$ to decay into a photon due to momentum conservation. Exciton polaritons with $k < \kappa$, on the other hand, exhibit the radiative width due to such a decay; it is reflected in the imaginary part of Σ in Fig. 1(b). Moreover this width is greatly enhanced in comparison with localized emitters [37]. Following the numerical estimates in Ref. [23], magnitude η would be assessed as $\sim$0.75 eV Å, resulting in substantial contributions to the exciton dispersion. With this estimate, the energy unit used in Figs. 1(a) and 1(b) becomes $2\eta\kappa \sim 1.5$ meV for $\kappa \sim 0.01$ nm^{-1}. It is worthwhile to stress that this value agrees well with the intrinsic radiative linewidth of excitons in WSe_2 extrapolated from experiments in Ref. [43].

Because of the intervalley coupling J_1, the valley excitations are clearly not the eigenstates of the system. Instead, the eigenstates are their linear combinations $\Psi_{\pm} = 2^{-1/2}\begin{pmatrix} 1 \\ \pm\exp(-2i\theta) \end{pmatrix}$ that diagonalize matrix $\mathbf{\Sigma}$ and yield the corresponding self-energy corrections as

$$\Sigma_{\pm} = J_0 \pm J_1 = -2i\eta \times \begin{cases} \sqrt{\kappa^2 - k^2}, & (L), \\ \kappa^2/\sqrt{\kappa^2 - k^2}, & (T). \end{cases} \tag{17}$$

These eigenstates have, respectively, longitudinal, for Ψ_+, and transverse, for Ψ_-, polarizations with respect to polariton wave vector $\mathbf{k}$ [23]: for propagation along the x axis, e.g., Eq. (13) shows that the Ψ_+ combination corresponds to the transition moment $\propto (\mathcal{D}, +i\mathcal{D}) + (\mathcal{D}, -i\mathcal{D})$ along x while Ψ_- to the moment $\propto (\mathcal{D}, +i\mathcal{D}) - (\mathcal{D}, -i\mathcal{D})$ along y. The functional forms of self-energy corrections (17) for the free-standing monolayer are shown in Figs. 1(a) and 1(b) by dashed lines.

It is instructive to look at the electrostatic limit ($\kappa \to 0$) of the derived corrections: the intervalley component (16) then becomes $J_1 = \eta k$, precisely the result derived in Ref. [23]. Importantly, the intravalley component J_0 (15) becomes equal to J_1 in this limit. (This equality is also illustrated in direct calculations with the exchange Coulomb interaction in Sec. IV below.) It is then clear that in the electrostatic limit, only the L excitons would acquire the additional term $\Sigma_+ = 2\eta k$ in their dispersion due to long-range exchange interactions, while the dispersion of T excitons would remain unchanged ($\Sigma_- = 0$) as in Eq. (1); see a sketch in Fig. 1(c). This of course agrees with the basic electrostatics of transverse polarization waves. One concludes that no Dirac-cone-like behavior takes place even in the electrostatic limit. In the valley-centric basis this conclusion thus follows from the simultaneous account of both inter- and intravalley processes as opposed to the intervalley coupling alone that was originally used in Ref. [23] (but see Ref. [29]).

III. EXCITON POLARITONS FROM MACROSCOPIC MAXWELL EQUATIONS

The results obtained in Sec. II for polaritonic eigenstates agree with the picture known for quantum wells [33] and basically reflect the fact that the opposite-handedness in-plane susceptibilities χ_1 and χ_2 of the individual valleys just add up in the overall *isotropic* electrodynamic response of the monolayer. The latter is then characterized by the scalar susceptibility χ defining the monolayer 2D current density $\mathbf{j} = -4\pi i\omega\chi\mathbf{E}$ induced by the in-plane electric field $\mathbf{E}$. It is this current density that enters the boundary conditions for the macroscopic Maxwell equations determining the effects of long-range fields on the system excitations [31,37]. For well-separated excitonic states [Eq. (1)], e.g., the 2D scalar susceptibility acquires a familiar single-oscillator form

$$\chi(\omega,k) = \chi_0 + A/\left[\omega_0^2(k) - \omega^2 - 2i\gamma\omega\right], \tag{18}$$

where χ_0 is the background term due to higher frequency transitions and γ the phenomenological dissipation parameter. A many-oscillator form could be used instead of Eq. (18) to

include even more specifics for different TMD monolayers as determined, e.g., from experimental data.

The macroscopic framework is versatile and can be easily applied to various environments. Here we exemplify this by considering the model of an infinitesimally thin planar monolayer between two nonmagnetic media with dielectric constants ε_1 and ε_2. One can solve directly for the eigenfrequencies of the system. Alternatively, as is also useful for the problem of energy transfer in Sec. V, one looks at the poles of the reflection coefficients for electromagnetic waves in our sandwich configuration. The 3D setup involves not only the in-plane components of the fields and wave vectors but also their z components perpendicular to the planar interface. With the boundary conditions of the polarizable interface monolayer [44], one easily derives the reflection coefficient amplitudes for p- and s-polarized waves as (ω,k) dependent:

$$r^{(p)} = \left(\frac{\varepsilon_2}{k_{z2}} - \frac{\varepsilon_1}{k_{z1}} - 4\pi i\chi\right)\left(\frac{\varepsilon_2}{k_{z2}} + \frac{\varepsilon_1}{k_{z1}} - 4\pi i\chi\right)^{-1} \quad (19)$$

and

$$r^{(s)} = (k_{z1} - k_{z2} + 4\pi i\kappa^2\chi)(k_{z1} + k_{z2} - 4\pi i\kappa^2\chi)^{-1}. \quad (20)$$

The normal components $k_{zi} = (\varepsilon_i\kappa^2 - k^2)^{1/2}$ of the waves in the respective media appear, as usual [45], related to the in-plane wave number k for given frequency $\omega = c\kappa$. The in-plane component of the electric field in a p-polarized wave is along the in-plane wave vector $\mathbf{k}$ whereas in an s-polarized wave they are perpendicular to each other. Hence, the poles of Eq. (19) determine the dispersion and decay of the L polaritons while the poles of Eq. (20) those of the T polaritons. Writing the pole equations in the form

$$-\frac{1}{\chi} = -4\pi i \times \begin{cases} (\varepsilon_1/k_{z1} + \varepsilon_2/k_{z2})^{-1}, & (L), \\ \kappa^2/(k_{z1} + k_{z2}), & (T), \end{cases} \quad (21)$$

one recognizes that the functional dependence in the right-hand side of Eq. (21) reduces to that in Eq. (17) for the free-standing monolayer. It is also clear that with the negligible dissipation and screening due to higher frequency transitions, $-1/\chi \simeq 2\omega_0[\omega - \omega_0(k)]/A$ becomes just proportional to the self-energy corrections in the vicinity of the resonance, $\omega \simeq \omega_0$. The derivation with the effective dipole-dipole interactions thus fully agrees with the macroscopic electrodynamics result, and we obtain $A = 2\omega_0\eta/\pi\hbar$ by comparing Eqs. (17) and (21). Note that the screening by the surrounding media can substantially affect the exciton radius and binding energy, thereby reducing "the strength" A of the resonance of Eq. (18); the corresponding evaluations of exciton binding are outside of our scope in this paper.

Figures 1(a) and 1(b) illustrate the differences in the behavior of self-energy corrections for two systems: the symmetric sandwich with $\varepsilon_1 = \varepsilon_2 = 1$ (a free-standing monolayer) and the asymmetric sandwich with $\varepsilon_1 = 1$ and $\varepsilon_2 = 2.25$ (glasslike substrate), as follows from Eq. (21). It is transparent that in the symmetric case, the T-polariton branch exhibits splitting at the light cone, $k \to \kappa$, as consistent with the divergence of the radiative decay rate [Eq. (17)] at $k \to \kappa - 0$. Qualitatively different for the asymmetric sandwich, there is no divergence in the decay rate and the dispersion of the T-polariton branch is continuous. Figure 1(b) also shows the extension of the region of the radiative decay: polaritons with $\kappa < k < \sqrt{\varepsilon_2}\kappa$ can now decay into photons that propagate only in the substrate. Beyond that region, however, the intrinsic (without scattering effects) polaritons become nonradiative and, conversely, cannot be directly excited by plane-wave photons incident on the monolayer from the infinity—the situation similar to the excitation of surface waves such as surface plasmons [36,37,45].

IV. INTER- AND INTRAVALLEY EXCHANGE COULOMB INTERACTIONS

While we already discussed the exchange Coulomb corrections to exciton dispersion in Secs. II and III as the electrostatic limit of the full electromagnetic interactions, it is instructive to compare the inter- and intravalley contributions to the monolayer excitons via the direct evaluation of the exchange Coulomb effects of Eq. (5). The setup for the calculation was provided in Sec. II. Using Eqs. (4), (6), (7), and (10), the exchange matrix elements are straightforwardly calculated in the macroscopic (long-range part of the interaction) limit as

$$U^{\rm exch}_{\alpha\beta}(\mathbf{k}) = U_C(\mathbf{k})|\phi(0)|^2\left(\mathbf{k}\cdot\mathbf{d}^{\alpha}_{cv}\right)\left(\mathbf{k}\cdot\mathbf{d}^{\beta}_{vc}\right)/e^2, \quad (22)$$

where the 2D Fourier transform

$$U_C(\mathbf{k}) = \int d\mathbf{r}\, e^{i\mathbf{k}\cdot\mathbf{r}} U_C(\mathbf{r}).$$

For the uniformly screened Coulomb interaction, $U_C(\mathbf{k})/e^2 = 2\pi/\varepsilon k$.

With assignment (13) of the transition dipole matrix elements, one immediately finds that for the intravalley processes, $\alpha = \beta$,

$$\left(\mathbf{k}\cdot\mathbf{d}^{\alpha}_{cv}\right)\left(\mathbf{k}\cdot\mathbf{d}^{\beta}_{vc}\right) = k^2\mathcal{D}^2.$$

For the intervalley matrix elements, $\alpha \neq \beta$, one derives

$$\left(\mathbf{k}\cdot\mathbf{d}^{\alpha}_{cv}\right)\left(\mathbf{k}\cdot\mathbf{d}^{\beta}_{vc}\right) = k^2\mathcal{D}^2\exp(\pm 2i\theta),$$

depending on α. Thus, the energy correction matrix (22) acquires the form of Eq. (14), where

$$J_0 = J_1 = \eta k/\varepsilon. \quad (23)$$

As already mentioned above, this is precisely the electrostatic limit of full electromagnetic couplings (15) and (16), where the dielectric constant $\varepsilon = 1$ [the electrostatic limit of the case considered in Sec. III would lead to Eq. (23) for $\varepsilon_1 = \varepsilon_2 = \varepsilon$].

The direct evaluation of the exchange corrections confirms that the intravalley processes are as important for the resulting dispersion of excitons as the intervalley processes are. The basic electrostatics tells us that there are no macroscopic charge densities associated with transverse polarization waves (polarization $\mathbf{P}$ perpendicular to wave vector $\mathbf{k}$), hence there should be no electrostatic corrections to the T-exciton energies. In the valley-centric framework, this necessitates $J_0 = J_1$ as indeed derived in calculations.

V. APPLICATION TO ENERGY TRANSFER

While photons cannot couple to nonradiative modes, the direct excitation of such modes is possible by the near electromagnetic fields, a particularly well-known example

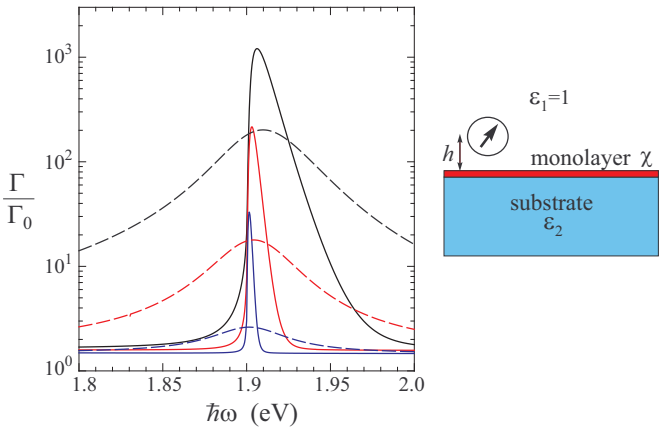

FIG. 2. (Color online) Acceleration of the decay rate Γ of a randomly oriented electric dipole emitter such as a quantum dot in the vicinity of the monolayer on a glasslike substrate as compared to the spontaneous decay rate Γ_0 in vacuum. The data computed with Eq. (24) are shown as a function of the emitter frequency ω and for different distances h to the interface: 5 nm (black lines), 10 nm (red), and 20 nm (blue). Solid lines display results for the nearly dissipationless excitons ($\gamma = 0.1$ meV), dashed lines are for the dissipation parameter $\gamma = 25$ meV. These illustrative calculations were done with the model parameters $4\pi\chi_0 = 2$ nm, $4\pi\hbar^2 A = 0.25$ eV^2 nm in Eq. (18) and $\hbar\omega_0 = 1.9$ eV, $M_0 = m_e$ in Eq. (1).

being the excitation of surface plasmons. This may be accomplished, e.g., with special optical geometry setups [36,37,45] or via resonance energy transfer (ET) from proximal quantum emitters such as molecules or quantum dots [45–47]. It should be noted that ET from 0D emitters to (quasi) 2D absorbers has been of increasing theoretical and experimental interest, including organic and inorganic semiconductors [48], graphene [49], and MoS_2 [38,39] (see also references therein). As ET provides a new decay channel, it is thus manifested experimentally in the acceleration of the observed emitter's photoluminescence decay.

Using the macroscopic electrodynamics formalism developed for such applications [45,47], the decay rate Γ of the randomly oriented electric-dipole emitter in the medium with dielectric constant ε_1 at distance h from the planar interface (see the sketch in Fig. 2) is derived [45] as

$$\Gamma/\Gamma_1 = 1 + \left(1/2k_1^3\right) \mathrm{Re} \int_0^\infty (k\,dk/k_{z1})\, e^{2ik_{z1}h} \times \left[\left(2k^2 - k_1^2\right) r^{(p)} + k_1^2 r^{(s)}\right], \quad (24)$$

where Γ_1 is the spontaneous decay rate in the uniform medium and $k_1^2 = \varepsilon_1\kappa^2$. The integration in Eq. (24) over *all* values of the in-plane wave vectors k signifies that the near fields of the emitter are included. Figure 2 illustrates the results computed with Eq. (24), where the reflection coefficients (19) and (20) were used as appropriate for the geometry sketched in the figure. The analysis shows that a very large effect observed in Fig. 2 is predominantly due to the excitation of L polaritons (related to poles of $r^{(p)}$), similar to a very efficient excitation of surface plasmons by ET [46,47]; the dispersion of the peak with distance h is also clearly seen.

With the numerical estimates used in Sec. II one would obtain $4\pi\hbar^2 A \sim 1.1$ eV^2 nm for the resonance strength A in Eq. (18). Keeping in mind a possible screening by the substrate, the illustration in Fig. 2 was computed with a more moderate value of the parameter A, its larger values would lead to even faster ET into the monolayer. It is worth pointing out that ET via the excitation of exciton polaritons takes place already with the vanishing dissipation parameter $\gamma \to 0$. Figure 2, however, also shows how the narrower polariton peaks are spread by the exciton damping. Excitation of TMD monolayer polaritons via high-efficiency ET from neighboring emitters might be attractive for various optoelectronic applications [38,39,50]. The acceleration of decay of quantum dot excitons due to ET into monolayer and multilayer MoS_2 has been recently observed experimentally [38,39].

VI. FINAL REMARKS

The main discussion in this paper has been focused on the effects of long-range electromagnetic interactions on the properties of *intrinsic* exciton polaritons in TMDs. We have shown that these effects result in the generic behavior characteristic of excitons in 2D systems with the isotropic in-plane macroscopic polarizability. While TMDs are specific in the nature of their valley-centric basis for bare excitons with the opposite-handed circular polarization, the proper account of intra- and intervalley long-range interactions "restores" the overall isotropic macroscopic response. Thanks to the substantial exciton binding, TMDs appear attractively positioned to study the dynamics of excitons as enabled by both the electron-hole motion and the long-range electromagnetic interactions.

While the choice of the "natural" exciton basis is not consequential for the effects that we discussed here, it may become important for the appropriate treatment of other types of interactions. In particular, it is understood that various scattering and dephasing processes such as those due to polariton interactions with phonons and defects can significantly affect the observable optical properties of real TMDs. The important issue of exciton decoherence is recognized [43] and will likely continue to be actively explored. The availability of high-quality TMD samples should assist in the studies of the intrinsic properties at low temperatures.

As we discussed in Sec. II, the long-range spatial coherence of 2D exciton polaritons within the light cone is expected to result in their shortened radiative lifetimes. The observations of picosecond-scale decay of photoluminescence [39] may be already indicative of a high degree of coherence but even subpicosecond intrinsic radiative lifetime was deduced from extrapolation of the experimental data [43]. That extrapolated intrinsic radiative linewidth of $\sim$1 meV agrees well with our estimates for the radiative linewidth of polaritons in Sec. II. The low-temperature studies of the radiative decay may contribute to assessing the polariton dispersion: Just as with the quantum well polaritons, their thermalization can lead to a specific temperature dependence of the radiative lifetime. With the substantial contribution to polariton dispersion in TMDs from the long-range interactions we discussed, that temperature dependence would deviate from the dependence resulting from the purely parabolic exciton dispersion [51].

A more direct experimental analysis of the subtleties of the exciton-polariton dispersion and decay exemplified in Fig. 1 should be achievable with experiments involving angle-resolved reflectivity and resonance photoluminescence, similar to experiments employed in Ref. [32] that uncovered the formation of cavity polaritons with MoS_2.

The dispersion of excitons well beyond the light cone is essentially driven by electrostatic interactions and expected to be less sensitive to long-range spatial coherence. The experimental techniques developed to study various surface exciton polaritons [52], such as attenuated total reflection, should prove to be useful. The macroscopic electrodynamics framework that we discussed in this paper would provide the connection to such experiments. Finally, detailed studies of energy transfer from neighboring quantum emitters into TMD-containing structures as a function of different emitter frequencies, distances, and substrates could also be used for quantification of exciton and polariton properties.

ACKNOWLEDGMENTS

Y.N.G. is grateful to NSF for the support provided through the DMR-1207123 grant. X.L. and C.Z. are supported by ARO (W911NF-12-1-0334) and AFOSR (FA9550-13-1-0045).

[1] A. K. Geim and I. V. Grigorieva, Van der Waals heterostructures, Nature **499**, 419 (2013).

[2] X. Xu, W. Yao, D. Xiao, and T. F. Heinz, Spin and pseudospins in layered transition metal dichalcogenides, Nat. Phys. **10**, 343 (2014).

[3] K. F. Mak, C. Lee, J. Hone, J. Shan, and T. F. Heinz, Atomically Thin MoS_2: A New Direct-Gap Semiconductor, Phys. Rev. Lett. **105**, 136805 (2010).

[4] D. Xiao, G.-B. Liu, W. Feng, X. Xu, and W. Yao, Coupled Spin and Valley Physics in Monolayers of MoS_2 and Other Group-VI Dichalcogenides, Phys. Rev. Lett. **108**, 196802 (2012).

[5] H. Zeng, J. Dai, W. Yao, D. Xiao, and X. Cui, Valley polarization in MoS_2 monolayers by optical pumping, Nat. Nanotech. **7**, 490 (2012).

[6] K. F. Mak, K. He, J. Shan, and T. F. Heinz, Control of valley polarization in monolayer MoS_2 by optical helicity, Nat. Nanotech. **7**, 494 (2012).

[7] T. Cao, G. Wang, W. Han, H. Ye, C. Zhu, J. Shi, Q. Niu, P. Tan, E. Wang, B. Liu, and J. Feng, Valley-selective circular dichroism of monolayer molybdenum disulphide, Nat. Commun. **3**, 887 (2012).

[8] J. S. Ross, S. Wu, H. Yu, N. J. Ghimire, A. M. Jones, G. Aivazian, J. Yan, D. G. Mandrus, D. Xiao, W. Yao, and X. Xu, Electrical control of neutral and charged excitons in a monolayer semiconductor, Nat. Commun. **4**, 1474 (2013).

[9] Y. Zhang, T.-R. Chang, B. Zhou, Y.-T. Cui, H. Yan, Z. Liu, F. Schmitt, J. Lee, R. Moore, Y. Chen, H. Lin, H.-T. Jeng, S.-K. Mo, Z. Hussain, A. Bansil, and Z.-X. Shen, Direct observation of the transition from indirect to direct bandgap in atomically thin epitaxial $MoSe_2$, Nat. Nanotech **9**, 111 (2014).

[10] K. F. Mak, K. He, C. Lee, G. H. Lee, J. Hone, T. F. Heinz, and J. Shan, Tightly bound trions in monolayer MoS_2, Nat. Mater. **12**, 207 (2013).

[11] J. Feng, X. Qian, C.-W. Huang, and J. Li, Strain-engineered artificial atom as a broad-spectrum solar energy funnel, Nat. Photon. **6**, 866 (2012).

[12] D. Lagarde, L. Bouet, X. Marie, C. R. Zhu, B. L. Liu, T. Amand, P. H. Tan, and B. Urbaszek, Carrier and Polarization Dynamics in Monolayer MoS_2, Phys. Rev. Lett. **112**, 047401 (2014).

[13] K. F. Mak, K. L. McGill, J. Park, and P. L. McEuen, The Valley Hall effect in MoS_2 transistors, Science **344**, 1489 (2014).

[14] B. W. H. Baugher, H. O. H. Churchill, Y. Yang, and P. Jarillo-Herrero, Intrinsic electronic transport properties of high-quality monolayer and bilayer MoS_2, Nano Lett. **13**, 4212 (2013).

[15] X. Li, F. Zhang, and Q. Niu, Unconventional Quantum Hall Effect and Tunable Spin Hall Effect in Dirac materials: Application to an Isolated MoS_2 Trilayer, Phys. Rev. Lett. **110**, 066803 (2013).

[16] R.-L. Chu, X. Li, S. Wu, Q. Niu, W. Yao, X. Xu, and C. Zhang, Valley-splitting and valley-dependent inter-Landau-level optical transitions in monolayer MoS_2 quantum Hall systems, Phys. Rev. B **90**, 045427 (2014).

[17] A. M. Jones, H. Yu, J. S. Ross, P. Klement, N. J. Ghimire, J. Yan, D. G. Mandrus, W. Yao, and X. Xu, Spin–layer locking effects in optical orientation of exciton spin in bilayer WSe_2, Nat. Phys. **10**, 130 (2014).

[18] G. Aivazian, Z. Gong, A. M. Jones, R.-L. Chu, J. Yan, D. G. Mandrus, C. Zhang, D. Cobden, W. Yao, and X. Xu, Magnetic control of valley pseudospin in monolayer WSe_2, Nat. Phys. **11**, 148 (2015).

[19] A. M. Jones, H. Yu, N. J. Ghimire, S. Wu, G. Aivazian, J. S. Ross, B. Zhao, J. Yan, D. G. Mandrus, D. Xiao, W. Yao, and X. Xu, Optical generation of excitonic valley coherence in monolayer WSe_2, Nat. Nanotech. **8**, 634 (2013).

[20] S. Wu, J. S. Ross, G.-B. Liu, G. Aivazian, A. Jones, Z. Fei, W. Zhu, D. Xiao, W. Yao, D. Cobden, and X. Xu, Electrical tuning of valley magnetic moment through symmetry control in bilayer MoS_2, Nat. Phys. **9**, 149 (2013).

[21] D. Y. Qiu, F. H. da Jornada, and S. G. Louie, Optical Spectrum of MoS_2: Many-Body Effects and Diversity of Exciton States, Phys. Rev. Lett. **111**, 216805 (2013).

[22] F. Hüser, T. Olsen, and K. S. Thygesen, How dielectric screening in two-dimensional crystals affects the convergence of excited-state calculations: Monolayer MoS_2, Phys. Rev. B **88**, 245309 (2013).

[23] H. Yu, G. Liu, P. Gong, X. Xu, and W. Yao, Bright excitons in monolayer transition metal dichalcogenides: From Dirac cones to Dirac saddle points, Nat. Commun. **5**, 3876 (2014).

[24] G.-B. Liu, W.-Y. Shan, Y. Yao, W. Yao, and D. Xiao, Three-band tight-binding model for monolayers of group-VIB transition metal dichalcogenides, Phys. Rev. B **88**, 085433 (2013).

[25] T. C. Berkelbach, M. S. Hybertsen, and D. R. Reichman, Theory of neutral and charged excitons in monolayer transition metal dichalcogenides, Phys. Rev. B **88**, 045318 (2013).

[26] G. Berghauser and E. Malic, Analytical approach to excitonic properties of MoS_2, Phys. Rev. B **89**, 125309 (2014).

[27] A. Ramasubramaniam, Large excitonic effects in monolayers of molybdenum and tungsten dichalcogenides, Phys. Rev. B **86**, 115409 (2012).

[28] F. Wu, F. Qu, and A. H. MacDonald, Exciton band structure of monolayer MoS_2, Phys. Rev. B **91**, 075310 (2015).

[29] H. Yu, X. Cui, X. Xu, and W. Yao, Valley excitons in two-dimensional semiconductors, Natl. Sci. Rev. **2**, 57 (2015).

[30] P. K. Basu, *Theory of Optical Processes in Semiconductors, Bulk and Microstructures* (Clarendon, Oxford, 1997).

[31] H. Haug and S. W. Koch, *Quantum Theory of the Optical and Electronic Properties of Semiconductors* (World Scientific, Singapore, 2004).

[32] X. Liu, T. Galfsky, Z. Sun, F. Xia, E. Lin, Y. Lee, S. K. éna-Cohen, and V. M. Menon, Strong light-matter coupling in two-dimensional atomic crystals, Nat. Photon. **9**, 30 (2015).

[33] L. C. Andreani and F. Bassani, Exchange interaction and polariton effects in quantum-well excitons, Phys. Rev. B **41**, 7536 (1990).

[34] R. Girlanda, S. Savasta, and B. Azzerboni, Quantum description of the electromagnetic field in a confined polarizable medium, Riv. Nuovo Cim. **21**, 1 (1998).

[35] A shorter version of this paper is available as an eprint: Y. N. Gartstein, X. Li, and C. Zhang, Exciton polaritons in transition-metal dichalcogenides and their direct excitation via energy transfer, arXiv:1502.00905.

[36] V. M. Agranovich and V. L. Ginzburg, *Crystal Optics with Spatial Dispersion, and Excitons* (Springer, Berlin, 1984).

[37] V. M. Agranovich, *Excitations in Organic Solids* (Oxford University, Oxford, 2009).

[38] F. Prins, A. J. Goodman, and W. A. Tisdale, Reduced dielectric screening and enhanced energy transfer in single- and few-layer MoS_2, Nano Lett. **14**, 6087 (2014).

[39] D. Prasai, A. R. Klots, A. K. M. Newaz, J. S. Niezgoda, N. J. Orfield, C. A. Escobar, A. Wynn, A. Efimov, G. K. Jennings, S. J. Rosenthal, and K. I. Bolotin, Electrical control of near-field energy transfer between quantum dots and two-dimensional semiconductors, Nano Lett. **15**, 4374 (2015).

[40] J. D. Jackson, *Classical Electrodynamics* (Wiley, New York, 1975).

[41] Y. N. Gartstein and V. M. Agranovich, Excitons in long molecular chains near the reflecting interface, Phys. Rev. B **76**, 115329 (2007).

[42] The real part of the diagonal elements $\Sigma_{\alpha\alpha}$ in integral (11) would formally diverge with interaction (12) due to the short-distance $\propto 1/r^3$ behavior of the electrostatic dipole-dipole coupling. There is no divergence, however, in the off-diagonal elements. Of course, at short distances the point-dipole description does not apply, whereas the actual short-range Coulomb interactions would be determined by the detailed behavior of electron wave functions. The divergent electrostatic term needs therefore to be separated in the calculation. The separated term corresponds to a k-independent shift $\Sigma_0\delta_{\alpha\beta}$ in the self-energy matrix and represents an overall renormalization of the exciton energies due to short-range interactions that we are not interested in.

[43] G. Moody, C. K. Dass, K. Hao, C. Chen, L. Li, A. Singh, K. Tran, G. Clark, X. Xu, G. Bergauser, E. Malic, A. Knorr, and X. Li, Intrinsic exciton linewidth in monolayer transition metal dichalcogenides, arXiv:1410.3143.

[44] We restrict our attention here to the layer with the in-plane polarizability only. When taking into account the polarizability perpendicular to the layer, the expression for the reflection coefficient $r^{(p)}$ is more involved than Eq. (19).

[45] L. Novotny and B. Hecht, *Principles of Nano-Optics* (Cambridge University, Cambridge, England, 2006).

[46] M. R. Philpott, Effect of surface plasmons on transitions in molecules, J. Chem. Phys. **62**, 1812 (1975).

[47] R. R. Chance, A. Prock, and R. Silbey, Molecular fluorescence and energy transfer near interfaces, in *Advances in Chemical Physics*, Vol. 37, edited by S. A. Rice and I. Prigogine (Wiley, New York, 1978), p. 1.

[48] J. M. Gordon and Y. N. Gartstein, Dielectric polarization, anisotropy and nonradiative energy transfer into nanometre-scale thin semiconducting films, J. Phys.: Condens. Matter **25**, 425302 (2013).

[49] L. Gaudreau, K. J. Tielrooij, G. E. D. K. Prawiroatmodjo, J. Osmond, F. J. G. de Abajo, and F. H. L. Koppens, Universal distance-scaling of nonradiative energy transfer to graphene, Nano Lett. **13**, 2030 (2013).

[50] V. M. Agranovich, Y. N. Gartstein, and M. Litinskaya, Hybrid resonant organic-inorganic nanostructures for optoelectronic applications, Chem. Rev. **111**, 5179 (2011).

[51] J. Feldmann, G. Peter, E. O. Göbel, P. Dawson, K. Moore, C. Foxon, and R. J. Elliott, Linewidth Dependence of Radiative Exciton Lifetimes in Quantum Wells, Phys. Rev. Lett. **59**, 2337 (1987).

[52] *Surface Polaritons*, edited by V. M. Agranovich and D. L. Mills (North Holland, Amsterdam, 1982).